Journal of Sciences, Islamic Republic of Iran 31(4): 357 - 368 (2020) http://jsciences.ut.ac.ir
University of Tehran, ISSN 1016-1104

In vivo and *In vitro* Biocompatibility Study of Fe_3O_4@ZnO and Fe_3O4@SiO_2 as Photosensitizer for Targeted Breast Cancer Drug Delivery

E. Naderi[1], M. Naseri[2], H. Taimouri Rad[3], R. Zolfaghari Emameh[4], Gh. Farnoosh[3], R. Ali Taheri[1*]

[1] *Nanobiotechnology Research Center, Baqiyatallah University of Medical Sciences, Tehran, Islamic Republic of Iran*
[2] *Department of Physics, Malayer University, Malayer, Islamic Republic of Iran*
[3] *Biotechnology Research Center, Baqiyatallah University of Medical Sciences, Tehran, Islamic Republic of Iran*
[4] *Department of Energy and Environmental Biotechnology, National Institute of Genetic Engineering and Biotechnology (NIGEB), 14965/161, Tehran, Islamic Republic of Iran*

Received: 25 August 2020 / Revised: 29 September 2020 / Accepted: 1 November 2020

Abstract

The present study aimed to prepare Fe_3O_4 nanocarriers (NCs) by a thermal treatment method. After the Fe_3O_4 (Fe) NCs was prepared, zinc oxide and silica nanoparticles were added to it as Photosensitizer. The structure, morphology, and magnetic properties of Fe_3O_4@ZnO (Fe@Zn) and Fe_3O_4@SiO_2 (Fe@Si) NCs were determined by XRD, FT-IR, FESEM, and VSM. Then, the loading and drug release of Fe, Fe@Zn, and Fe@Si NCs were investigated**.** The curcumin (CUR) release of Fe@Zn+CUR and Fe@Si+CUR increased from 30% and 26% at pH 7.4 to 53% and 57% at pH 5.5, respectively. The cytotoxicity of Fe@Zn and Fe@Si NCs were determined by MTT assay, hemolysis test, acute toxicity, and lethal dose test. The results showed that Fe@Zn and Fe@Si were appropriate for Photodynamic Therapy (PDT) and in the next step, the effect of Fe@Zn, Fe@Si, Fe@Zn+CUR, and Fe@Si+CUR NCs on MCF-7 cells under visible light were studied. Finally, the ranking of the destruction of cancerous cells of MCF-7 using NCs under visible light was: Fe@Zn+CUR>Fe@Zn>Fe@Si+CUR>Fe@Si.

Keywords: Photosensitizer; Drug Delivery; Curcumin; Cytotoxicity; Magnetic properties.

Introduction

Iron oxide nanoparticles are widely applicable in drug delivery, photodynamic therapy (PDT), magnetic hyperthermia, magnetic fluids, enzyme immobilization, Magnetic resonance imaging, magnetic bio-separation, nanoadsorption, and catalysis [1-5]. They are very useful in drug delivery because of improving targeting, having low toxicity, being bioavailable, and having suitable magnetic properties. Breast cancer is extremely dangerous and its treatment is a challenge for researchers because of tumors resistance to drug

* Corresponding author: Tel: +989126110865; Fax: +98 2188617712; Email: taheri@bmsu.ac.ir

absorption [6]. To treat this type of cancer, there are several ways (radiotherapy, chemotherapy, and surgery) that have numerous side effects. One of the novel and effective methods for cancer treatment is photodynamic therapy (PDT) that is a method of non-invasive with limited side effects. Photodynamic therapy involves the destruction of cancer cells through combining light and photosensitizer. The use of some nanoparticles in photodynamic therapy allows for maintaining the stability of the photosensitizer before reaching cancer cells and the targeted delivery of more photosensitizer molecules to the tumor area [7-11]. The combination of PDT with other methods can improve the effects of the PDT and also remove its side elects. Drug delivery is a useful method that can help the drug to be distributed more appropriately, be released under more control, be more stable, and more bioavailable [12-16]. In this research, iron oxide nanoparticles were prepared via the thermal-treatment method. This method is an easy and comfortable technique for fabrication of ferrite nanoparticles. Then, zinc oxide and silica nanoparticles were added to the Fe_3O_4 matrix. After adding curcumin (CUR) to Fe_3O_4@ZnO (Fe@Zn) and Fe_3O_4@SiO_2 (Fe@Si) as NCs (Fe@Si), rate of release, capacity of loading, biocompatibility. Also, their properties in drug delivery and PDT were checked. Finally, the effect of Fe@Zn, Fe@Si NCs as Photosensitizer in the presence and absence of drug on MCF-7 cells were investigated.

Materials and Methods

Materials

1-(4, 5-Dimethylthiazol-2-yl)-3, 5-diphenyl formazan (Aldrich, St. Louis, USA, CAS. 57360-69-7), CUR (Merck, Art No. 820354), Deionized water was synthesized by an ultra-pure water system (Smart-2-Pure, TKACO, Germany). PVP (Mw=29000), Fe $(NO_3)_3.9H_2O$, Ca $(NO_3)_2$. $6H_2O$ was provided by Sigma Aldrich. The other chemicals and solvents were also provided in purity grades by chemical lab.

Preparation of Fe_3O_4 nanoparticles

Iron oxide nanoparticles were prepared by a thermal-treatment method [17]. 3.5g polyvinyl pyrrolidone (PVP) was dissolved in 100 ml of distilled water and then, 0.2 mmol of iron (III) nitrate and 0.1 mmol of iron (II) nitrate were added to the polymer solution at 80 ºC. The resulting solution was stirred for 2h by a magnetic stirrer in order to achieve a clear solution. Then, it was dried for 24h at 90 ºC in an oven. The predecessor of the dried solid was crushed and ground in a mortar to form a powder. Finally, the powder was calcined at 500 ºC for 3h.

Preparation of Fe_3O_4@ZnO

0.05g of prepared Fe_3O_4 nanoparticles were dispersed in 100 ml of distilled water. After ultrasonic mixing for 30 min, 3.5 g of PVP was added to iron oxide nanoparticles suspension in turn under vigorous stirring at 80 °C. Then, 0.89g of zinc nitrate was added to the mixture while keeping the stirring speed. Then, the mixture was dried in an oven for 24 hours at 90 °C. The sample was milled and ground in a mortar to form a powder. Finally, the powder was calcined at 500 ºC for 3h [18].

Preparation of Fe_3O_4@SiO_2

0.35g of prepared Fe_3O_4 nanoparticles were dispersed in 24 mL of ethanol and water solution by ultrasonic cleaning bath. After ultrasonic mixing for 30 min, 0.8 ml of ammonia solution and 4 mL of tetraethyl orthosilicate (TEOS) were added to iron oxide in turn under vigorous stirring. The mixture was washed by ethanol and deionized water 4 times and finally dried at 80 °C for 7 h in an oven to prepare Fe_3O_4@SiO_2 [19].

Characterization

XRD patterns were obtained through X-ray diffraction measurements (XRD; Philips X-pert type instrument, Germany) by Cu Kα radiation (kα=1.54059 Å). The microstructure was characterized using a FESEM (Tescan Mira). Absorption modes of NCs were obtained using FT-IR spectra. The magnetic properties of the samples were checked by VSM (Lake Shore 4700).

Drug loading

Drug loading was done by a precipitation method. 10 mg of NCs was dispersed in 25 mL of deionized water. Then 3 mg of CUR dispersed in 2 mL of acetone was drop-wisely added to it under vigorous stirring at room temperature. Eventually, the sample was washed four times and dried at room temperature [20]. Figure 1 shows the schematic view of all steps of tumor destruction by Photosensitizer.

Preparation of release and drug loading

1 mg of drug-loaded NCs were immersed in acetone and then the amount of the drug loading and encapsulation efficiency in the supernatant solutions was measured by UV-Vis spectrophotometer (GENESYSTM 10S, λ_{max} =420 nm). The drug loading (DL %) and drug adsorption (DA %) are calculated using equations (1) and (2), respectively:

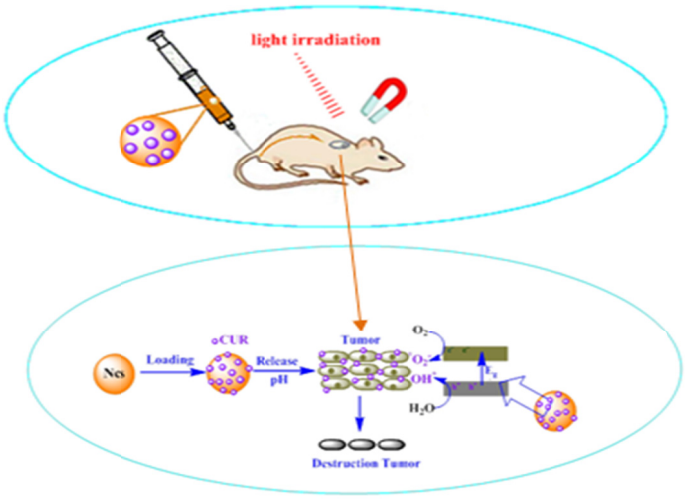

Figure 1. A schematic illustration of tumor destruction by prepared NCs under light irradiation.

$$DL(\%) = \frac{W_{loaded\ drug}}{W_{loaded\ drug} + W_{carrier}} \times 100 \quad (1)$$

$$DA(\%) = \frac{W_{loaded\ drug}}{W_{total\ drug}} \times 100 \quad (2)$$

Where $W_{loaded\ drug}$, $W_{carrier}$, and $W_{total\ drug}$ are the weight of loaded CUR, carrier weight, and drug total weight.

In vitro release of the drug

For in vitro release of the drug, 1 mg of the drug-loaded NCs was immersed into 10 mL of phosphate buffer saline (PBS) (containing 1% tween 80) at 37°C with mild stirring (Heidolph Titramax 1000). Experiments were performed at pH 7.4 and 5.5 to simulate normal tissue and tumor tissue media. Finally, the amount of the released drug in the supernatant solutions was calculated at a given period by the UV-Vis spectrophotometer at 420 nm.

Hemolysis Test

The estimation of the toxicity of a sample for blood is measured by the hemolysis assay test. The samples of heparinized blood were centrifuged at 4000 rpm for 5 minutes. After washing the remaining RBCs using PBS and RBCs, the solution was synthesized with a certain ratio (RBC: PBS=1:20). Then, 0.5 mL of NCs (10 mg/mL) and 0.5 mL of the prepared RBCs solution were added to tubes. These tubes were put at a shaker for 4 h (37 ± 1 °C). Finally, the percentage of hemolysis was calculated by UV–Vis spectrophotometry [20]. This test was carried out three times.

$$Hemolysis\ (\%) = \frac{A_{sample} - A_{negative}}{A_{positive} - A_{negative}} \times 100 \quad (3)$$

The hemolysis is measured with Equation (3), where A_{sample}, $A_{negative}$, and $A_{positive}$ are sample absorbance, PBS absorbance and deionized water absorbance, respectively.

Cell Cytotoxicity

Cytotoxicity of NCs was estimated by 3-[4, 5-dimethylthiazol-2-yl]-2, 5-diphenyl tetrazolium bromide (MTT) assay. HEK-293 (normal cell) and MCF-7 (cancer cell) cells were incubated with 96-well plate (10^4 cells per well) for 24 h. They contained 100µL of DMEM with 15% (v/v) FBS and 1% penicillin/streptomycin. Different concentrations (13.8-69.8µg/mL) of NCs irradiated by a high-pressure 250W Hg lamp for 20 min were added to test cells and afterward, the cells were cultured for another 48 h. Then, 20µl of MTT solution was added to each well. After 4h, this solution was replaced with 100µL of dimethyl sulfoxide to dissolve formazan crystals. Finally, the absorbance was evaluated at 570 nm.

Lethal Dose

10 male mice (35 – 40 g) were taken from laboratory. For the test the weight of all mice was checked out, then mice were given by 550mg/kg oral dose. The physical changes in all mice were studied for 6 h. After 24 h, if the animals survive, the dose would be administered to two additional mice, if additional mice survive, the experiment would be finished. Otherwise, other animals are selected for determination of lethal dose.

Furthermore, the changing of the mice weight were checked out for one week because changing of weight is an important factor in to determine toxicity of nanocarriers [20].

Results and Discussion

Structure and morphology of NCs

The typical XRD pattern of Fe_3O_4 nanoparticles, Fe_3O_4@ZnO and Fe_3O_4@SiO_2 NCs are shown in Figure 2. The structure of the cubic spinel of ferrite iron corresoponded with the standard pattern (ICDD PDF: 00-039-0238, Ie3m space group) (Fig.2a). The diffraction planes of (200), (104), (110), (321) and (224) corresponded to the phase formed Fe_3O_4 (magnetite) and the diffraction planes (024), (116) and (300) were related to the α-Fe_2O_3 phase (hematite). Hematite phase presence in iron oxide nanoparticles is caused by the thermal-treatment method. The presence of ZnO nanoparticles in the sample is confirmed because of the accordance of the XRD pattern of zinc oxide (Reference Code: 01-080-007, P63mc space group) with a hexagonal phase (Fig.2b). Reduction of the intensity of X-ray diffraction in Figure 2c was assigned to the amorphous silica (Reference code: 01-086-2326), indicating the formation of Fe_3O_4@SiO_2 nanocomposite.

Figures 3a to 3d shows the FTIR spectrum of Fe@Zn, Fe@Zn+CUR, Fe@Si, Fe@Si+CUR nanocomposites, respectively. The absorption bands at 434.28 and 548.54 cm^{-1} for Fe@Zn are attributed to Zn−O and Fe−O bonds (Figure .3a). These absorption bands shifted to 458.24 and 540.25 cm^{-1} for Fe@Zn+CUR [21]. The absorption peaks at 405.61 and 589.09 cm^{-1} for Fe@Si are attributed to Fe−O and Si−O−Fe bonds (Figure .3c), peaks of which shifted to 458.24 and 573.42 cm^{-1} for Fe@Si+CUR [22]. The absorption peak of 704.27 cm^{-1} was observed at both Fe@Zn and Fe@Si, that is related to C−N=O band which transferred from 704.27 to 712.56 cm^{-1} for Fe@Zn+CUR. The absorption peaks at 1088.51 and 810.23 cm^{-1} for Fe@Si corresponded to the bending mode of Si–O–Si which transferred from 1088.51 to 1096.8 cm^{-1} for Fe@Si+CUR. The absorption bands at 850.7 (Fe@Zn+CUR) and 859.7 cm^{-1} (Fe@Si+CUR) are associated with the benzoate trans–CH. The absorption mode of 957.67 cm^{-1} at Fe@Zn+CUR and Fe@Si+CUR is related to the peak of the enol C-O which arises from the presence of curcumin [18]. The absorption mode of 1391.67 cm^{-1} at Fe@Zn,

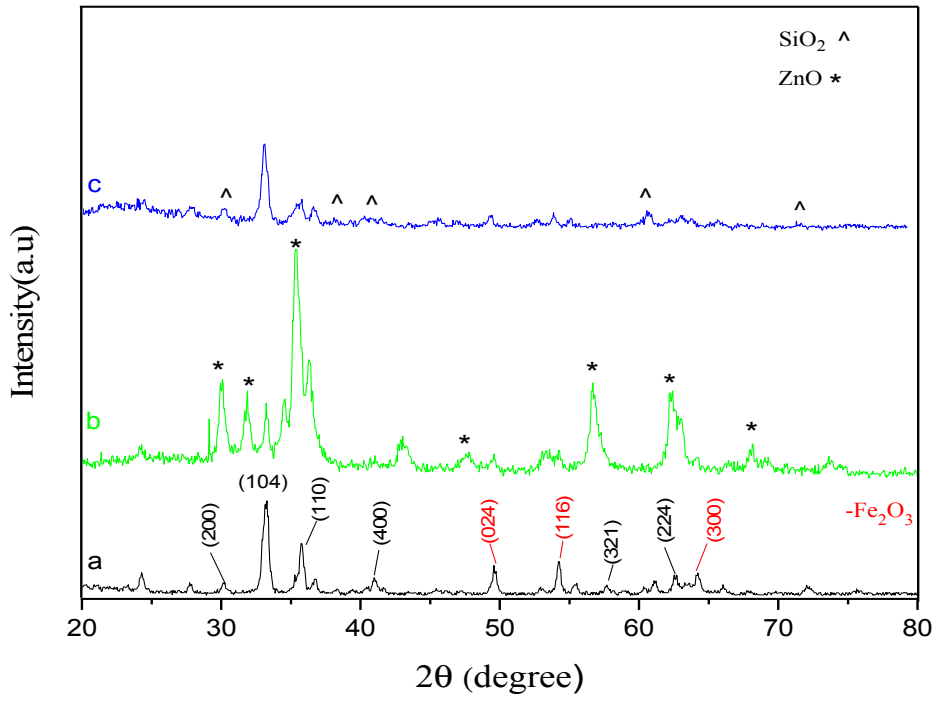

Figure 2. XRD patterns of (a) Fe, (b) Fe@Zn, (c) Fe@Si

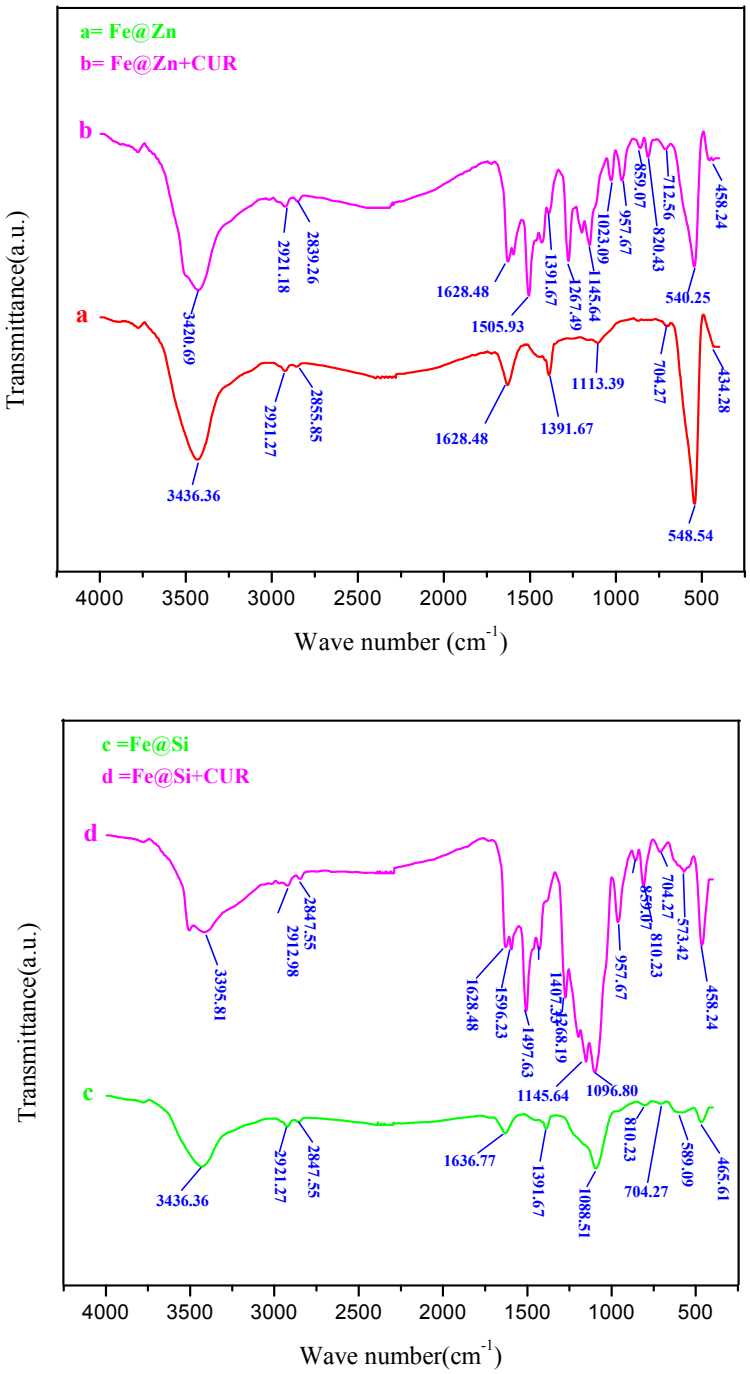

Figure 3. FT-IR spectra of (a) Fe@Zn, (b) Fe@Zn+CUR, (c) Fe@Si, (d) Fe@Si+CUR

Fe@Zn+CUR and Fe@Si is related to C-H which transferred from 1391.67 to 1407.33 cm^{-1} for Fe@Si+CUR. The stretching vibration 1628.48 cm^{-1} at all samples is related to C=C. With the addition of curcumin, absorption bands of 1055.93 and 1596.23 cm^{-1} were appeared at Fe@Zn+CUR and Fe@Si+CUR, respectively. The peaks 2839 to 2930 cm^{-1} in all samples (a to d) were resulted from the asymmetric C−H stretching. The bending vibrations at the range 3395 to 3440 cm^{-1} are associated with O–H [23-25].

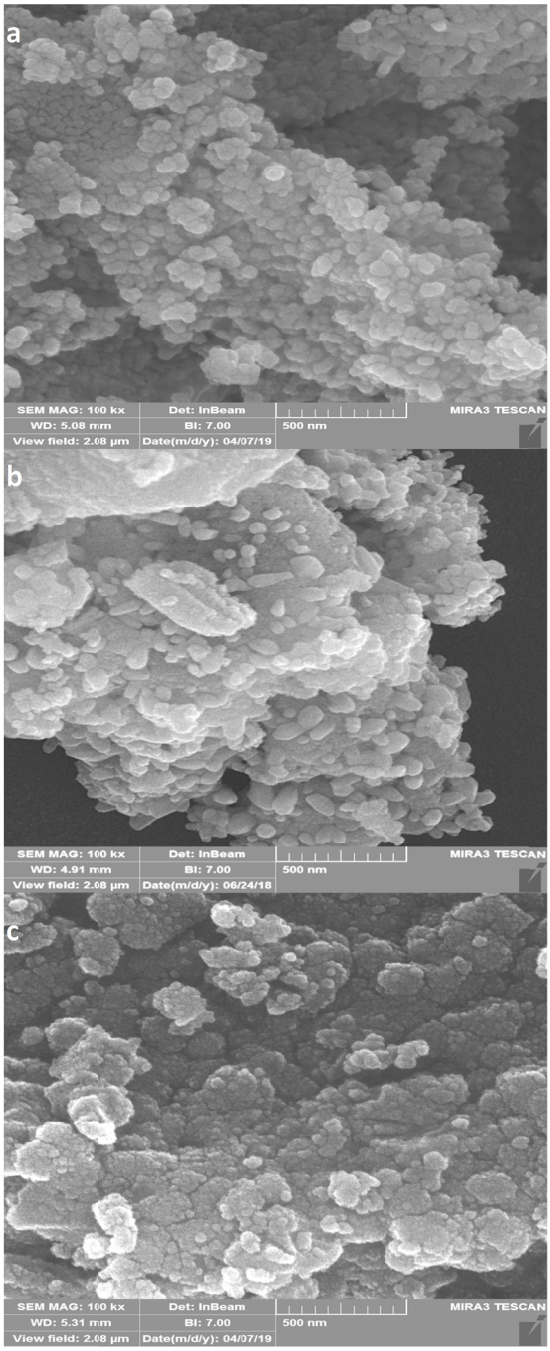

Figure 4. FESEM images of (a) Fe, (b) Fe@Zn, (c) Fe@Si.

FESEM of Fe_3O_4 nanoparticles, Fe_3O_4@ZnO and Fe_3O_4@SiO_2 NCs are shown in Figure 4. As can be seen, the average diameters of Fe, Fe@Zn, and Fe@Si NCs were estimated to be 23, 42, and 65 nm, respectively. The appearance of zinc oxide and silica added to iron oxide increased the average diameters of samples. Fe nanoparticles and Fe@Si nanocomposite were distributed in a nearly uniform, spherical shape. The existence of some agglomerated areas in iron Fe@Zn NCs is the result of using the thermal-treatment method.

Magnetic properties

The typical magnetization curves vs. magnetic field for Fe, Fe@Zn, and Fe@Si NCs were depicted in Figure 5. The results were summarized in Table 1. Results of

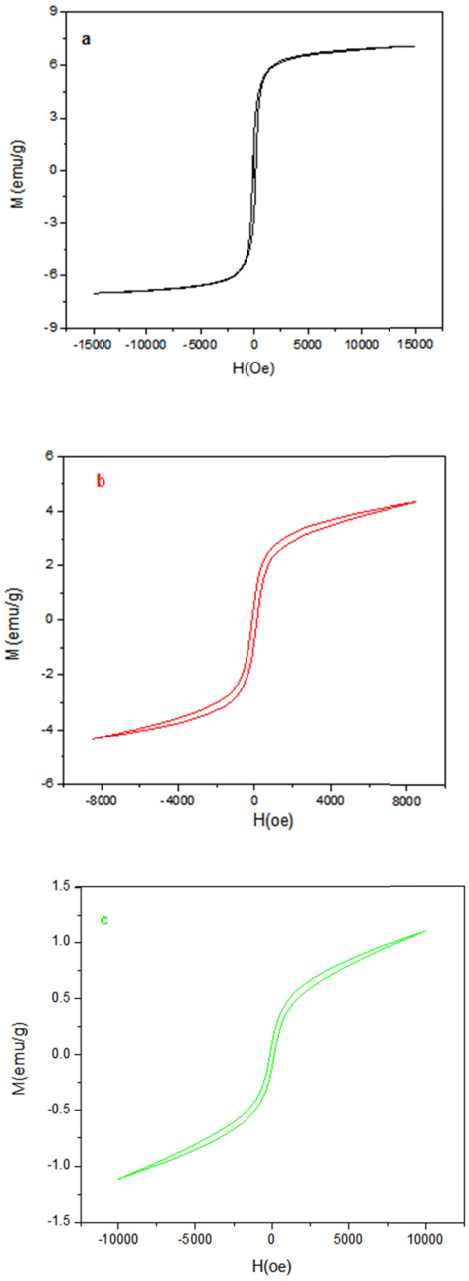

Figure 5. Hysteresis loops of (a) Fe, (b) Fe@Zn, (c) Fe@Si

Table 1. Results of VSM analysis

Nanocarriers	Saturation Magnetization (M_s) (emu/g)	Coercivity Field H_c (Oe)	Remanent Magnetization (M_r) (emu/g)	Remanence ratio ($R=M_r/M_s$)
Fe_3O_4(Fe)	7.11	143.88	2.21	0.31
Fe@Zn	4.34	102.38	1.07	0.24
Fe@Si	1.10	151.92	0.11	0.1

VSM analysis showed that Fe, Fe@Zn, and Fe@Si NCs had ferromagnetic behaviors. Fe nanoparticles exhibited a low saturation magnetization of 7.11emu/g, which can be resulted from the coexistence of hematite and magnetite phases in the sample. After with the addition of zinc oxide and silica to iron oxide, values of saturation magnetization (M_s), coercivity (H_c), and remained magnetization (M_r) changed to 4.34, 1.1emu/g, 102.38, 151.92Oe, and 1.07, 0.11emu/g, respectively. Saturation magnetization in these samples decreased compared with iron oxide nanoparticles because of the presence of diamagnetic protective layer at the surface of bare nanoparticles. After the silica was added to bare nanoparticles, H_C increased suddenly, indicating the presence of a magnetically dead layer that reduced the response of changes in the magnetic particles to the magnetic field [22]. Since R<0.5, the interaction of domains in this material is related to the interaction of magnetostatic [25].

Study of drug loading and release

The amounts of drug loading and adsorption in Fe, Fe@Zn, and Fe@Si NCs are shown in Table 2. Drug loading efficiency and adsorption efficiency of Fe@Zn, Fe@Si NCs were much higher than that of Fe, which could be related to the interaction of the strong π-π stacking between shells and curcumin [26, 27]. Curcumin was absorbed on the silica surface by forming a bond with the silanol groups (Si–OH). Increased drug loading of Fe@Si compared with that of Fe@Zn can be attributed to the porous surface of the mesoporous silica shell [5, 28]. The profiles of CUR release from Fe@Zn and Fe@Si NCs at different pH are presented in Figure 6. The CUR release rate of Fe@Si+CUR was gradual and persistent at pH 7.4, which can be attributed to the absorption of CUR in NCs mesoporous. As can be seen

Table 2. Drug loading of NCs

Nanocarriers	Nanocarriers weight (mg)	CUR weight (mg)	Loading CUR (w/w %)	Adsorption CUR (w/w %)
Fe	10	3	13.56 ± 1.36	52.36 ± 6.11
Fe@Zn	10	3	20.07 ± 0.54	83.75 ± 2.86
Fe@Si	10	3	22.34 ± 0.16	95.90 ± 0.91

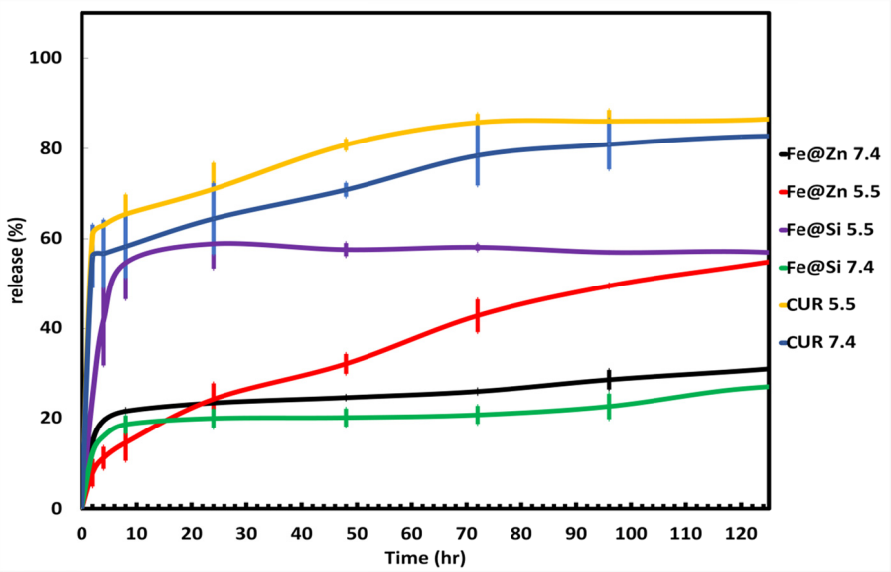

Figure 6. Release rate at pH 5.5 and 7.4.

in Figure 6, the CUR release rate obviously increased with the decrease of pH from 7.4 to 5.5. After 24 h, the release rate at Fe@Si NCs was much higher than that of Fe@Zn NCs. CUR release after 120 h at pH 5.5 for Fe@Zn NCs and Fe@Si NCs were 53% and 57%, respectively. Results indicate that release of CUR at various pH depends on the interaction of hydrogen bondings and the electrostatic interaction between NCs and CUR [26, 27]. Therefore, appropriate NCs can be prepared for delivering drugs to cancerous cells.

The Study of hemolysis test

The hemolytic activity of NCs was displayed in Table 3. It was clearly seen that the hemolytic activity increased by adding zinc oxide and silica to the Fe matrix. Since zinc ion was slightly toxic, the hemolytic activity in Fe@Si was less than that of Fe@Zn [18]. Nevertheless, Fe@Zn and Fe@Si NCs in this test displayed acceptable biocompatibility and appropriate amount of the hemolysis (lower than 5%).

The Study of the effect of nanocarriers on normal and cancer cells

The cytotoxicity of Fe@Zn and Fe@Si NCs in normal cells of HEK-293 were estimated by a MTT test. As seen in Figure 7, Fe@Zn and Fe@Si NCs cell viability at 67.5µg/mL concentration were 59 % and 86 %, respectively. Also, Table 4 demonstrates analysis of statistical related to Figure 7. The results indicate that cell viability is reduced through increasing the concentration of NCs. Cell activity of Fe@Si is more than that of Fe@Zn that can be attributed to the presence of zinc oxide on the cells. Findings show that zinc oxide nanoparticles compared to their bulk have intrinsic preferential cytotoxicity against cancer cells [28, 29]. Since the media is neutral, cell viability at 45µg/mL increases from 63 % to 80 % by loading the CUR on the surface of zinc oxide nanoparticles. The effect of Fe@Zn, Fe@Si, Fe@Zn+CUR, and Fe@Si+CUR on cancer cells of MCF-7 under light irradiation are shown in Figure 8.

Also, Table 5 demonstrates analysis of statistical related to Figure 8. As seen, the destruction of cancer cells increases with an increase in the concentration of Fe@Zn and Fe@Si under light irradiation due to the interaction of photosensitizer NCs with cancer cells. Because the band gap energy of Fe@Zn (E_g~2.30eV) is more than that of Fe@Si (E_g~3.27eV), less energy is required to transfer electrons from the valence band to the conduction band [30, 31]. Thus, most of the

Table 3. Hemolysis percent of NCs.

Sample	Sample Code	Concentration (mg/mL)	Hemolysis 10 (mg/mL)
Fe	1	10	0.27 ± 0.02
Fe@Zn	2	10	4.68 ± 1.42
Fe@Si	3	10	3.54 ± 0.84

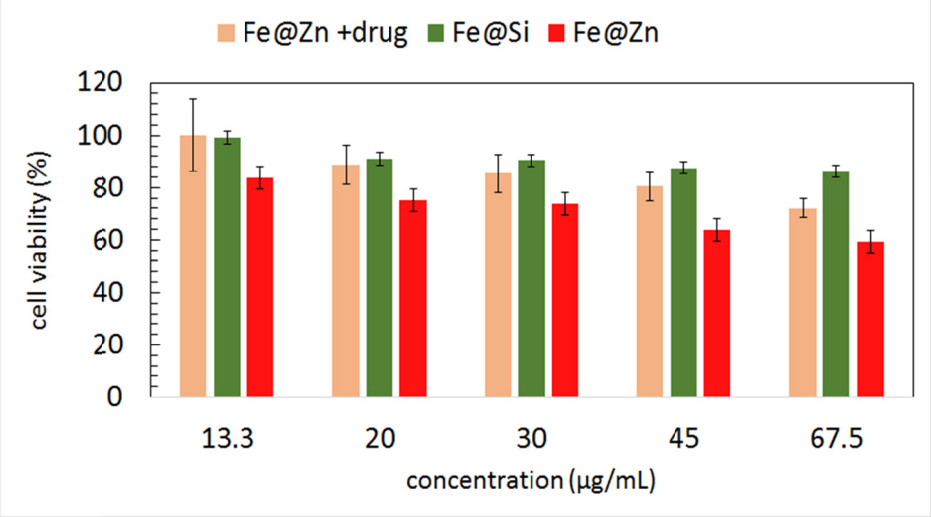

Figure 7. Cell viability of NCs on HEK-293 cell lines after 72 h

Table 4. Statistical analysis related to Figure 7

Concentration (µg/mL)	Tukey's multiple comparisons test	Significant?	Adjusted P Valu
13.3	Fe@Zn+drug vs. Fe@Si	No	0.9903
	Fe@Zn+drug vs. Fe@Zn	Yes	0.019
	Fe@Si vs. Fe@Zn	Yes	0.026
20	Fe@Zn+drug vs. Fe@Si	No	0.9156
	Fe@Zn+drug vs. Fe@Zn	No	0.0515
	Fe@Si vs. Fe@Zn	Yes	0.0207
30	Fe@Zn+drug vs. Fe@Si	No	0.6626
	Fe@Zn+drug vs. Fe@Zn	No	0.1027
	Fe@Si vs. Fe@Zn	Yes	0.0148
45	Fe@Zn+drug vs. Fe@Si	No	0.4338
	Fe@Zn+drug vs. Fe@Zn	Yes	0.0156
	Fe@Si vs. Fe@Zn	Yes	0.0006
67.5	Fe@Zn+drug vs. Fe@Si	Yes	0.0473
	Fe@Zn+drug vs. Fe@Zn	No	0.0744
	Fe@Si vs. Fe@Zn	Yes	0.0001

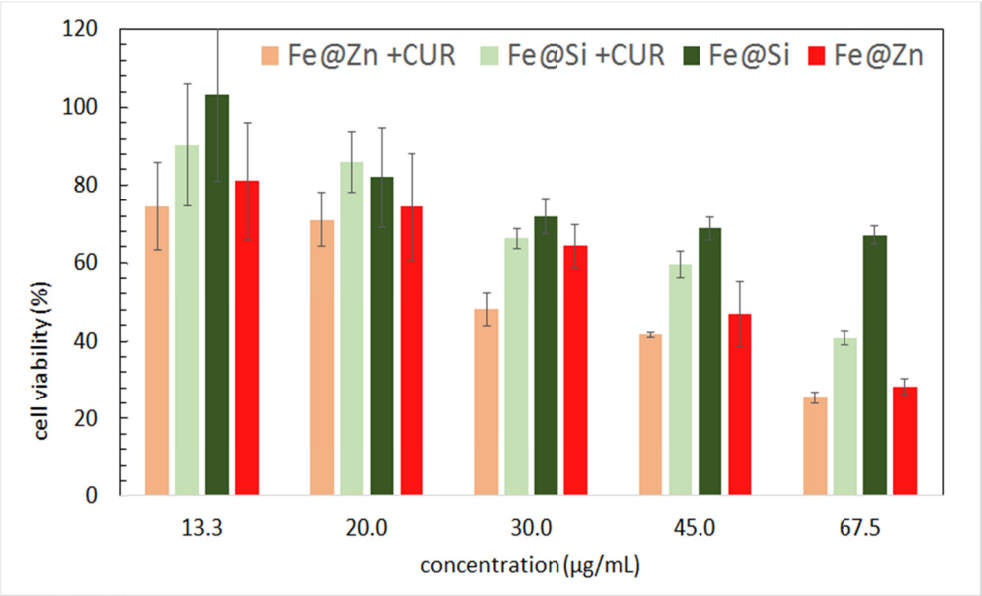

Figure 8. Cell viability of NCs on MCF-7 cell lines after 72 h under light irradiation

electrons are excited from the conduction band (CB) to the valence band (VB). As a result, Reactive Oxygen Species (ROS) in the media increased by increasing the number of electrons in CB and the holes in VB. When the concentration of NCs increases to 67.5µg/mL, the activity of cancer cells decreases, a phenomenon that can be attributed to the increase in ROS production which is resulted from increased NCs concentration [32, 33]. According to Figure 8, the destruction of cancer cells is mostly related to loading of CUR on Fe@Zn NCs under light irradiation. Although loading and releasing of Fe@Zn is less than that of Fe@Si, the results indicate that the destruction of cancerous cells using Fe@Zn+CUR under visible light are more than those destructed by Fe@Si+CUR, revealing the effect of photosensitizers NCs on cancer cells of MCF-7.

Table 5. Statistical analysis related to Figure 8

Concentration (µg/mL)	Tukey's multiple comparisons test	Significant?	Adjusted P Value
13.3	Fe@Zn+CUR vs. Fe@Si+CUR	No	0.1296
	Fe@Zn+CUR vs. Fe@Zn	Yes	0.0006
	Fe@Zn+CUR vs. Fe@Si	Yes	0.0012
	Fe@Si+CUR vs. Fe@Zn	No	0.1832
	Fe@Si+CUR vs. Fe@Si	No	0.2717
	Fe@Zn vs. Fe@Si	No	0.9959
20	Fe@Zn+CUR vs. Fe@Si+CUR	No	0.1707
	Fe@Zn+CUR vs. Fe@Zn	Yes	0.0046
	Fe@Zn+CUR vs. Fe@Si	No	0.414
	Fe@Si+CUR vs. Fe@Zn	No	0.4475
	Fe@Si+CUR vs. Fe@Si	No	0.9481
	Fe@Zn vs. Fe@Si	No	0.1902
30	Fe@Zn+CUR vs. Fe@Si+CUR	No	0.058
	Fe@Zn+CUR vs. Fe@Zn	Yes	<0.0001
	Fe@Zn+CUR vs. Fe@Si	Yes	0.0074
	Fe@Si+CUR vs. Fe@Zn	No	0.09
	Fe@Si+CUR vs. Fe@Si	No	0.8475
	Fe@Zn vs. Fe@Si	No	0.3883
45	Fe@Zn+CUR vs. Fe@Si+CUR	No	0.0614
	Fe@Zn+CUR vs. Fe@Zn	Yes	0.0452
	Fe@Zn+CUR vs. Fe@Si	Yes	0.0004
	Fe@Si+CUR vs. Fe@Zn	No	0.9992
	Fe@Si+CUR vs. Fe@Si	No	0.2595
	Fe@Zn vs. Fe@Si	No	0.3211
67.5	Fe@Zn+CUR vs. Fe@Si+CUR	No	0.1435
	Fe@Zn+CUR vs. Fe@Zn	No	0.4029
	Fe@Zn+CUR vs. Fe@Si	Yes	<0.0001
	Fe@Si+CUR vs. Fe@Zn	No	0.9274
	Fe@Si+CUR vs. Fe@Si	Yes	0.0026
	Fe@Zn vs. Fe@Si	Yes	0.0004

Acute Toxicity

All mice survived one week after the test. Furthermore, bodyweight change is directly related to the toxicity of NCs. After 24 h and one week, the mice weight increased normally, indicating the natural physical activity of all mice (Table 6). Therefore, it could be concluded that all NCs were safe.

Conclusion

The structure, morphology, and magnetic properties of zinc oxide and silica coated iron oxide NCs were studied. The results of VSM analysis showed that

Table 6. Weight changes after oral administration of 550mg/kg NCs

	Weight Changes after 24 h (%)	Weight Changes after a Week (%)
Control	2.0 ± 0.0	10.0 ± 0.0
Fe@Zn	1.0 ± 1.7	0.0 ± 2.9
Fe@Si	0.0 ± 0.0	4.8 ± 1.6

Fe, Fe@Zn, and Fe@Si NCs demonstrated ferromagnetic behaviors. The loading capacity of the drug increased with the addition of zinc oxide and silica nanoparticles to iron oxide matrix. The release of CUR was increased by decreasing pH from 7.4 to 5.5. The results of MTT assay, hemolysis test, lethal dose test and acute toxicity showed that the prepared Fe@Zn and Fe@Si are appropriate for Photodynamic Therapy (PDT). The ranking of the destruction of cancerous cells using Fe@Zn, Fe@Si, Fe@Zn+CUR, and Fe@Si+CUR NCs under light irradiation was known to be

Fe@Zn+CUR>Fe@Zn>Fe@Si+CUR>Fe@Si

Acknowledgement

The authors would like to thank from the "Clinical Research Development Center of Baqiyatallah hospital" for their kindly cooperation.

Funding

This study was funded by Baqiyatallah University of Medical Sciences. (Grant number 91003414)

Ethical approval

All applicable international, national, and institutional guidelines for the care and use of animals were followed. (Research ethics certificate approval ID: IR.BMSU.REC.1397.324, Approval date: 2019-03-04)

References

1. Lee N., D. Yoo, Ling D., Cho M.H., Hyeon T., Cheon J. Iron Oxide Based Nanoparticles for Multimodal Imaging and Magnetoresponsive Therapy. *J. Chem Rev.* **115**:10637-89 (2015).
2. Wei W., Zhaohui W., Taekyung Y., Changzhong J., Woo-Sik K. Recent progress on magnetic iron oxide nanoparticles: synthesis, surface functional strategies and biomedical applications. *J. Sci Technol Adv Mater.* **16**:023501 (2015).
3. Masoudi R. , Moghimi H., Azin E., Taheri A. Adsorption of cadmium from aqueous solutions by novel Fe_3O_4-newly isolated Actinomucor sp. bio-nanoadsorbent: functional group study,Artificial Cells. *J.Artificial Cells Nanom and Biot.* **46:**1092-1101 (2018).
4. Gupta R., Sharma D. Evolution of Magnetic Hyperthermia for Glioblastoma Multiforme Therapy. *J. ACS Chem. Neurosci.* **10:** 1157–1172 (2019).
5. Beg M. Sh., Mohapatra J., Pradhan L., Patkar D., Bahadur D. Porous Fe_3O_4-SiO_2 Core-Shell Nanorods as High-Performance MRI Contrast Agent and Drug Delivery Vehicle. *J. Mag and Mag Mat.* **428:** 340-347 (2017).
6. Kossatz S., Grandke J., Couleaud P., et al. Efficient treatment of breast cancer xenografts with multifunctionalized iron oxide nanoparticles combining magnetic hyperthermia and anti-cancer drug delivery. *J. Bre Cancer Res.* **17**:66 (2015).
7. Aghajanzadeh M., Naderi E., Zamani M., Sharafi A., Naseri , Danafar H. . In vivo and In vitro Biocompatibility Study of $MnFe_2O_4$ and $Cr_2Fe_6O_{12}$ as Photosensitizer for Photodynamic Therapy and Drug Delivery of Anti-Cancer Drugs. *J. Drug Dev and Indus Phar.* **29:**1-6 (2020).
8. McFarland Sh. A., Mandel A., Dumoulin-White R., Gasser G. Metal-based photosensitizers for photodynamic therapy: the future of multimodal oncology? *J. Cur Opin in Chem Bio*. 56:23-27 (2020).
9. Fan Y. Zhou T. Cui P. F., He .J, Chang. Xin, Xing L., Jiang H. Modulation of Intracellular Oxygen Pressure by Dual-Drug Nanoparticles to Enhance Photodynamic Therapy. *J. Adv Func Mater*. 29:1806708 (2019).
10. Li Sh., Shen X., Xu Q., Cao Y. Gold nanorod enhanced conjugated polymer /photosensitizer composite nanoparticles for simultaneous two-photon excitation fluorescence imaging and photodynamic therapy. J. Nanoscale. 11: 19551-19560 (2019).
11. Kazantzis K.T., Koutsonikoli K., Mavroidi B., Zachariadis M., Alexiou P., Pelecanou M., Politopoulos K., Alexandratou E., Sagnou M. Curcumin derivatives as photosensitizers in photodynamic therapy: photophysical properties and in vitro studies with prostate cancer cells. *J. Photochem & Photobio Sci*. 19:193-206 (2020).
12. Anselmo A. C., Mitragotri S. Impact of particle elasticity on particle-based drug delivery systems. *J. Advan drug deliv rev*. **108**: 51-67 (2017).
13. Torchilin V. P. stimuli-sensitive nanoparticulate systems for drug delivery. *J. Natu rev Drug dis.* **13:** 813 (2014).
14. Colilla M., Baeza A., Vallet, Regí M. Mesoporous silica nanoparticles for drug delivery and controlled release applications. *The SolGel Handbook*. 1309-1344 (2015).
15. Cheung K., Das D. B. Microneedles for drug delivery: trends and progress. *Drug deliv*. **23**:2338-2354 (2016).
16. Blanco E., Shen H., Ferrari M. Principles of nanoparticle design for overcoming biological barriers to drug delivery. *Natu biotec* . **33**:941 (2015).
17. Anajafi Z., Naseri M., Neri G., Acetone sensing behavior of p-$SmFeO_3$/n-ZnO nanocomposite synthesized by thermal treatment method. *J.Sensor and Actu B: Chem*. **304:**127252 (2020).
18. Zamani M., Naderi E., Aghajanzadeh M., et al. $Co_{1-x}Zn_xFe_2O_4$ based nanocarriers for dual-targeted anticancer drug delivery: Synthesis, characterization and in vivo and in vitro biocompatibility study. *J. Mole Liqu* . **274**: 60-67 (2019)
19. Naseri M., Kamalianfar A., Naderi E., Hashemi A. The effect of Ag nanoparticles on physical and photocatalytic properties of $ZnFe_2O_4$/SiO_2 nanocomposite. *J. Molecular structure.***1206:**127706 (2020).
20. Naderi E., Aghajanzadeh M., Zamani M., , Sharafi A. , Naseri M., Danafare H. The Effect of Calcination Temperature on the Anticancer Activity of $CaFe_2O_4$ @ PVA Nanocarriers: Photodynamic Therapy and Drug Delivery Study, *J .Inorganic and Organ Poly and Mater***. 20:**1-9 (2020).
21. Hosseini S. M., Monfared H. H., Abbasi V., Khoshroo M. R., Nanostructural Characterization of the

Fe_3O_4/ZnO Magnetic Nanocomposite as an Application in Medicine *J . Super and Nov Mag*. **30:** 3541-3548 (2017).
22. Naderi E., Naseri M.and Souri D.. The effect of SiO_2 and TiO_2 nanoparticles on physical properties of $SrFe_{12}O_{19}$ nanoparticle. *Current App Phy.* **18:** 469-476 (2018).
23. Naseri M., Naderi E., Sadrolhosseini A. R. Effect of Phase Transformation on Physical and Biological Properties of PVA/$CaFe_2O_4$ Nanocomposite. *J. Fib and Poly*. **17**: 1667-1674 (2016).
24. Chireh M., Naseri M. Effect of calcination temperature on the physical properties of $LiFe_5O_8$ nanostructures. *J. Adv Pow Tech*. **30**: 952-96022 (2019).
25. Naseri M., Ghasemi R. Structure and physical properties of Fe_6 O_8/ba Fe_6 O_{11} nanostructure. *Mag and Mag Mat*. **406**:200–206 (2016).
26. Zamani M., Rostami M., Aghajanzadeh M., Kheiri Manjili H., Rostamizadeh K., and Danafar H.. Abdelsalam. Mesoporous titanium dioxide@zinc oxide–graphene oxide nanocarriers for colon-specific drug delivery. *Mat Science.* **53:** 1634–1645 (2018).
27. Shen L., Li B., Qiao Y., and Song J. Monodisperse Fe_3O_4/SiO_2 and Fe_3O_4/SiO_2/PPy Core-Shell Composite Nanospheres for IBU Loading and Release. *Materials*. **12**: 823 (2019).
28. Qiu H., Cui B., Li G., Yang J., Peng H., Wang Y., Li N., Gao R., Chang Zh., Novel Fe_3O_4@ZnO@mSiO_2 Nanocarrier for Targeted Drug Delivery and Controllable Release with Microwave Irradiation. *J. Phy Chem C*. **118:** 14929-14937 (2014).
29. Katsumiti A., Arostegui I. , Oron M. , Gillil D., Valsami-Jones E., Cytotoxicity of Au, ZnO and SiO_2 NPs using in vitro assays with mussel hemocytes and gill cells: Relevance of size, shape and additives. *J. Nanotoxicology.* **10**:185-93 (2016).
30. Suresh D., Kumbar, Sagar M., Menon, Samvit G., Choudhari K. S., Santhosh C. Novel Magnetically Separable Fe_3O_4@ZnO Core–Shell Nanocomposite for UV and Visible Light Photocatalysis. *J. Adv Sci Lett*. **23**:1724-1729 (2017).
31. Mortazavi-DerazkolaS., Salavati-Niasar M. , Amiri O., Abbasi A. Fabrication and characterization of Fe_3O_4@SiO_2@TiO_2@Ho nanostructures as a novel and highly efficient photocatalyst for degradation of organic pollution. *J. Ene Chem.* **26**: 17-23 (2017).
32. Zhu H., Li J., Qi X., Chen P. Orcid Oxygenic Hybrid Semiconducting Nanoparticles for Enhanced Photodynamic. *J. Therapy Nano Lett.* **18**: 1586-594 (2018).
33. Naderi E., Aghajanzadeh M., Zamani M., Hashiri A., Sharafi A., Kamalianfard A., Naseri M, Danafare H. Improving the anti-cancer activity of quercetin-loaded $AgFeO_2$ through UV irradiation: Synthesis, characterization, and in vivo and in vitro biocompatibility study. *J. Drug Del Sci and Tech.* **57**: 101645 (2020).